


Towards Dynamic Transparency: Robust Interaction Force Tracking Using Multi-Sensory Control on an Arm Exoskeleton

Conference Paper

Author(s):

[Zimmermann, Yves](#) ; Küçüktabak, Emek Baris; Farshidian, Farbod; Riener, Robert; [Hutter, Marco](#) 

Publication date:

2020

Permanent link:

<https://doi.org/10.3929/ethz-b-000466461>

Rights / license:

[In Copyright - Non-Commercial Use Permitted](#)

Originally published in:

<https://doi.org/10.1109/IROS45743.2020.9341054>

Towards Dynamic Transparency: Robust Interaction Force Tracking Using Multi-Sensory Control on an Arm Exoskeleton

Yves Zimmermann^{1,2}, Emek Barış Küçüktabak¹, Farbod Farshidian¹, Robert Riener^{2,†}, and Marco Hutter^{1,†}

Abstract—A high-quality free-motion rendering is one of the most vital traits to achieve an immersive human-robot interaction. Rendering free-motion is notably challenging for rehabilitation exoskeletons due to their relatively high weight and powerful actuators required for strength training and support. In the presence of dynamic human movements, accurate feedback linearization of the robot’s dynamics is necessary to allow for a linear synthesis of interaction wrench controllers. Hence, we introduce a virtual model controller that uses two 6-DoF force sensors to control the interaction wrenches of a multi-DoF torque-controlled exoskeleton over the joint accelerations and inverse dynamics. Furthermore, we propose a disturbance observer for controlling the joint acceleration to diminish the influence of modeling errors on the inverse dynamics. To provide a high-bandwidth, low-bias estimation of the system’s acceleration, we introduce a bias-observer which fuses the information from joint encoders and seven low priced IMUs. We have validated the performance of our proposed control structure on the shoulder and arm exoskeleton ANYexo. The experimental comparison of the controllers shows a reduction of the felt inertia and maximum reflected joint torque by a factor of more than three compared to state of the art. The controllers’ robustness w.r.t. a model mismatch is validated. The experiments show that the closed-loop acceleration control improves the tracking, particularly at joints with low inertia. The proposed controllers’ performance sets a new benchmark in haptic transparency for comparable devices and should be transferable to other applications.

I. INTRODUCTION

Physical human-robot interaction gained significance during the last years propelled by the increased fusion of robots into the human’s workplace. Many of these devices render haptic environments to the user. While robots dedicated to this task perform reasonably well, more universal devices often struggle to achieve the desired rendering fidelity. An epitome of this challenge is rehabilitation robots.

On the one hand, these devices should provide high-quality free motion (transparency) to avoid interfering with the patients’ movements while supporting them [1]. On the other hand, they need high torque actuation to allow for strength training, dynamic assessments [2], and to assist severely affected patients [3]. Limited transparency is acceptable for the first steps in therapy of severely affected patients [4], [5]. However, state-of-the-art devices strive to make robot-assisted therapy useful also for patients able to perform more

¹ Y. Zimmermann, E.B. Küçüktabak, F. Farshidian, and M. Hutter are with Robotic Systems Lab, ETH Zurich, Switzerland yvesz@ethz.ch

² Y. Zimmermann and R. Riener are with Sensory-Motor Systems Lab, ETH Zurich, Switzerland. R. Riener is additionally with Spinal Cord Injury Center, University Hospital Balgrist, Zurich, Switzerland riener@ethz.ch.

[†] R. Riener and M. Hutter contributed equally as lead of the project.

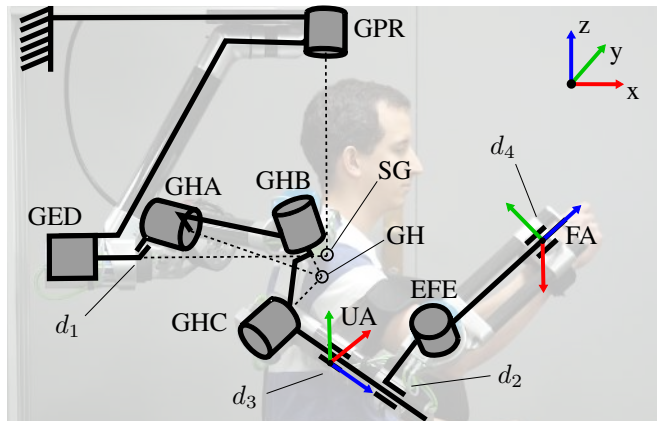


Fig. 1. The kinematic structure of the robot with the shoulder girdle joints (SG): protraction/retraction (GPR) and elevation/depression (GED); the glenohumeral joints (GH): GHA, GHB, and GHC; elbow joint (EFE); fixed passive link length adjustments d_i ; contact points upper arm (UA) and forearm (FA) with attached coordinate systems [6].

agile movements [6].

With these powerful and thus, bulky devices it is challenging to render haptic transparency for dynamic movements. *First*, often high transmission ratio gears are installed to achieve the required joint torques at reasonable weight and footprint. This design choice leads to increased joint friction and high reflected motor inertia at the joint [7]. Many state-of-the-art robots address this concern by series elastic actuation [2], [6], [8], [9]. *Second*, the mechanical impedance at the interaction point is comparatively large. Therefore, the non-linear dynamics should be compensated to control the device accurately. For trailing of fast human motions, vigorous control actions are required. Noise on the interaction force measurement, the actuator bandwidth, and controller sampling frequency limit the controller bandwidth. Hence advanced control designs have been proposed to improve the performance [10], [11]. Some devices have been developed with remote actuation to reduce the moving mass [12], [13]. However, due to the transmission, the bandwidth is further restricted, and additional non-linear friction is caused.

In this paper, we present a method to tackle the challenge mentioned above through a virtual model controller (VMC) using inverse dynamics (ID) for feedback linearization. We elaborate on the advantage of using the measured interaction wrench state for the linearization instead of the desired wrench when interacting with a soft, unknown impedance. To compensate errors in the ID model, we propose a closed-loop acceleration controller. This control method uses a multi-sensor signal with direct acceleration measurement as feedback. Further, we investigate the method’s performance

on the series elastic actuated exoskeleton ANYexo shown in Fig. 1.

II. SYSTEM DESCRIPTION

The hardware we use in this paper is a 6-DoF torque-controlled shoulder and arm exoskeleton designed as a research platform for methods concerning neural rehabilitation [6]. The device was developed with a focus on an extensive range of motion (ROM) and particularly activities that involve interaction with other parts of the user's body. Additional emphasis was put on swift motions to prevent limitation of speed recovery, as described in [6]. However, methods proposed in this paper should be transferable to any other torque controlled haptic device.

The device has two actuated DoF at the shoulder girdle (SG), three at the glenohumeral joint (GH), and one at the elbow, as shown in Fig. 1. There are two physical interaction points between user and robot: one at the upper arm (UA) and one at the forearm close to the wrist (FA).

Six series elastic actuators drive the robot. A forerunner version of these drives was presented in [14]. The version used for the experiments provides 40 N m peak torque at a bandwidth of 60 Hz at 3 N m amplitude and a resolution smaller than 0.1 N m. The maximum joint speed is 12 rad/s.

At both interaction points (UA/FA), there are 6-DoF force-torque sensors (Rokubi Mini 1.1 by Bota Systems) mounted. They provide force and torque measurements in a range of ± 1000 N and ± 8 N m in the x-direction and ± 500 N and ± 5 N m in the yz-plane with less than 0.02% noise. The integrated IMUs attached to the shell of the drives and the force-torque sensors provide inertial acceleration and angular velocities. Their properties are identified in section VI-A.

The controllers, state estimation, and the model description are updated at 800 Hz by a ROS and C++ based software stack. Control PC, actuators, and sensors communicate over an EtherCAT bus. The low-level torque controller for the SEA runs at 2.5 kHz on the integrated electronics of the drive.

A. Dynamics

The system of the human interacting with the robot is described in generalized coordinates by

$$\mathbf{M}_i(\mathbf{q}_i)\ddot{\mathbf{q}}_i + \mathbf{h}_i(\mathbf{q}_i, \dot{\mathbf{q}}_i) + \mathbf{g}_i(\mathbf{q}_i) = \mathbf{J}_{C,i}^\top(\mathbf{q}_i)\boldsymbol{\lambda}_C + \boldsymbol{\tau}_i, \quad (1)$$

where $i \in \{R, H\}$. Indices R and H denote the robot and human system respectively, \mathbf{q} are the generalized coordinates, \mathbf{M} is the mass matrix, \mathbf{h} the centrifugal and Coriolis terms, \mathbf{g} the gravitation terms, \mathbf{J}_C the stacked spatial Jacobian of the interaction points, $\boldsymbol{\tau}$ the joint torques, and $\boldsymbol{\lambda}_C$ the interaction wrench. For the high level control design, the actuators can be considered as perfect torque or position source within the bandwidths typical for humans that is around 7 Hz [6], [15]. Therefore, we assume

$$\boldsymbol{\tau}[k+1] = \Pi_{\text{ctrl}}(\mathbf{q}_R[k], \dot{\mathbf{q}}_R[k], \ddot{\mathbf{q}}_R[k], \boldsymbol{\lambda}_{C,\text{meas}}[k]), \quad (2)$$

where Π_{ctrl} is the control policy defining the target joint torque for the actuators and $\boldsymbol{\lambda}_{C,\text{meas}}$ is the measured interaction wrench.

The human H part of equation (1) is unknown regarding the parameters of the system dynamics as well as its exact state. The equations of motion (EoM) for R and H are only coupled over $\boldsymbol{\lambda}_C$. Therefore, we can model the human dynamics as unknown disturbance \mathbf{d}_H on the interaction wrench $\boldsymbol{\lambda}_C$. Therefore

$$\boldsymbol{\lambda}_C = \hat{f}_C(\mathbf{q}_R, \dot{\mathbf{q}}_R, \ddot{\mathbf{q}}_R, \mathbf{d}_H), \quad (3)$$

where \hat{f}_C is the unknown function describing the interaction depending on the relative motion of the interaction points.

B. Optimization Framework

We use a hierarchical null-space projection based optimization (HOC) as a standard on our hardware to manage safety relevant constraints and other tasks on different priorities [6], [16]. This method typically uses the following optimization vector $\boldsymbol{\xi} = (\ddot{\mathbf{q}}, \boldsymbol{\tau}, \boldsymbol{\lambda}_C)$.

The tasks \mathcal{T} are then defined as linear equality $\mathcal{T}_p : \mathbf{A}_p\boldsymbol{\xi} = \mathbf{b}_p$ or inequality $\mathcal{T}_p : \mathbf{D}_p\boldsymbol{\xi} \leq \mathbf{c}_p$ constraints at priority p , where small p means high priority. The equations of motion (1) and physical constraints should be defined on the first priority as a solution deviating from physics is never valid. The second priority can be used to define safety constraints and the lower priorities to set therapy relevant tasks, and regularization [6]. The next sections will discuss how to set the tasks for the HOC to track interaction wrenches.

III. ENVIRONMENT ANALYSIS

The optimal choice for an interaction force control method is highly dependent on the hardware and expected environment. *Admittance* controllers are generally used for systems that are primarily position-controlled (e.g., hydraulic actuated devices), *Impedance* controllers are used for systems with low impedance (e.g., pneumatics, SEA), and torque-controlled systems often use only feedforward control [17], [18], [19]. In this section, we explain why an admittance controller can be a better fit for a torque-controlled system in the presence of an environment with unknown low impedance, e.g., a human arm.

A. Environments with Known Impedance

Torque controlled robots offer a fairly easy method to control interaction wrenches towards a fixed environment (e.g., hard floor). In this case, all active contact DoF C can be assumed motionless $\dot{\mathbf{x}}_C, \ddot{\mathbf{x}}_C = \mathbf{0}$. This constraint allows projecting the EoM into the support consistent space. This assumption for fixed contact points is eligible for, e.g., legged robots, as they mostly assume a fixed and rigid floor [16], [11]. Also, for systems where the impedance of the environment at the interaction points is well known, the same method can be used. There the expected acceleration of the interaction point $\ddot{\mathbf{x}}_{C,\text{exp}}$ under the desired load $\boldsymbol{\lambda}_{C,\text{des}}$ can be estimated and compensated for by setting the equality task

$$\mathbf{J}_C\ddot{\mathbf{q}} = \ddot{\mathbf{x}}_{C,\text{exp}} - \dot{\mathbf{J}}_C\dot{\mathbf{q}}. \quad (4)$$

This task assures that all solutions of the HOC are chosen within the null-space of the support consistency constraint

(4). As next priority, the HOC receives the desired interaction wrench $\lambda_C = \lambda_{C,\text{des}}$ as an equality task and as last priority the regularization $\ddot{\mathbf{q}} = \mathbf{0}$. If no other tasks are defined, the optimal joint torque $\boldsymbol{\tau}^*$ to achieve the desired interaction wrench λ_C derives from equation (1)

$$\boldsymbol{\tau}^* = \mathbf{M}\ddot{\mathbf{q}}^* + \mathbf{h} + \mathbf{g} - \mathbf{J}_C^\top \lambda_{C,\text{des}}, \quad (5)$$

where $\ddot{\mathbf{q}}^*$ is the generalized acceleration resulting from the HOC. As we assumed perfect torque sources for our model, the desired interaction wrench would instantaneously be established. This means that on the non-perfect hardware the interaction wrench controlling task is converted to a joint torque control task without any loss in accuracy. Whereas the joint torque control performance is only dependent on the actuation system.

B. Environments with Unknown Impedance

For systems that interact with a mostly unknown environment like a human arm, it is not possible to estimate $\ddot{\mathbf{x}}_{C,\text{exp}}$. Without or with an inaccurate constraint (4) the torques from equation (5) do not establish the desired interaction wrench as the environment reacts unexpectedly to the robot's action. Consequently a deviation of the robot's acceleration from $\ddot{\mathbf{q}}^*$ occurs. Employing linear control synthesis for the interaction wrench tracking is sub-optimal due to the cross-coupling in the robot's wrench-acceleration dynamics.

IV. CONTROL APPROACH

As the model of the robot dynamics is significantly more accurate than the model of the environment, we suggest using all available information to define the robot's EoM as accurately as possible. Thereby at least the robot behaves as expected, even when coupled to a completely unknown environment. Furthermore, linear controller design is eligible as the feedback linearization is valid. Hence, we set the equality task $\lambda_C = \lambda_{C,\text{mes}}$ at the same priority as the EoM. This results in the best possible estimate of the real system dynamics at the time of the measurement. For rather low impedance environments as a human arm, this guess is also more accurate during the whole control cycle (i.e. after 1.25 ms) than assuming $\lambda_C = \lambda_{C,\text{des}}$. Thus the feedback linearization is as accurate as possible and only limited by the accuracy of the robot model and interaction force measurement. Hence, the system should track a desired accelerations task $\ddot{\mathbf{q}} = \ddot{\mathbf{q}}_{\text{des}}$ precisely as long as none of the safety constraints are active. In this case, the optimum joint torque is expressed by

$$\boldsymbol{\tau}^* = \mathbf{M}\ddot{\mathbf{q}}_{\text{des}} + \mathbf{h} + \mathbf{g} - \mathbf{J}_C^\top \lambda_{C,\text{mes}}. \quad (6)$$

Hence, we are looking for an admittance controller with desired accelerations as output.

A. Wrench Controller

In this paper, we demonstrate this strategy with a straight forward and easy to tune *virtual mass controller* (VMC). A good guess for the unknown environment's admittance is that it behaves as decoupled one-dimensional systems with

a mass that is attached to the robot via a spring-damper force element. Hence, accelerating the interaction points in the direction of the interaction wrench error $\lambda_{C,\text{err}} = \lambda_{C,\text{mes}} - \lambda_{C,\text{des}}$ will diminish the same. Large acceleration gains improve the tracking performance. However, a stable controller design is limited by the robots dynamics, actuation, and communication delay. The idea of the VMC is to schedule the acceleration gains so that the desired accelerations $\ddot{\mathbf{q}}_{\text{des}}$ mimic a desired virtual admittance under the influence of the residual interaction wrench error $\lambda_{C,\text{err}}$. We want to control a 12-DoF interaction wrench with six or less DoF of the exoskeleton. Therefore, we do not have full controllability over $\lambda_{C,\text{err}}$. Hence, we define the VMC in the generalized coordinates where the controllable part of the interaction wrench is mapped to the joint space. We propose to chose the virtual admittance so that it behaves like a down-scaled reflected inertia of the real robot system $\mathbf{M}_{\text{virt}} = \alpha \mathbf{M}_{\text{sys}}$. Where α is a tuning parameter. The robot's gravitational, centrifugal, and Coriolis terms can be compensated entirely without stability issues, as shown in [6]. Therefore, these terms are not included in the virtual admittance. The HOC obtains the desired joint accelerations $\ddot{\mathbf{q}}_{\text{des}}$ as an equality task

$$\ddot{\mathbf{q}}_{\text{des}} = \mathbf{M}_{\text{virt}}^{-1} \mathbf{J}_C^\top \lambda_{C,\text{err}} = \frac{1}{\alpha} \mathbf{M}_{\text{sys}}^{-1} \mathbf{J}_C^\top \lambda_{C,\text{err}}. \quad (7)$$

Due to the memoryless structure of the controller, this method is not prone to windup if a higher priority task is active on a subset of the controlled DoF. Hence, this free-motion controller can always be defined as a task of priority p_{VMC} . If other haptic interactions i should be modelled they can be added with a higher priority $p_i < p_{\text{VMC}}$. In this case, the haptic interaction i is rendered on its DoF while the VMC still controls the rest of the device's DoF.

To give an intuition about the feeling of this controller, we can investigate the admittance at joint level

$$\ddot{\mathbf{q}}_{\text{sys}} = \mathbf{M}_{\text{sys}}^{-1} \mathbf{J}_C^\top \left(\frac{1}{\alpha} \lambda_{C,\text{err}} + \Delta \lambda_C \right), \quad (8)$$

where $\Delta \lambda_C = (\lambda_{C,R} - \lambda_{C,\text{mes}})$ is the difference between the delay afflicted, measured interaction wrench $\lambda_{C,\text{mes}}$ and the continuous interaction force of the real system $\lambda_{C,R}$. Assuming a small delay and accurate measurement, this term gets negligible. Then the system behaves as a down-scaled impedance in the presence of $\lambda_{C,\text{err}}$.

B. Acceleration Tracking Controller

The inverse dynamics (ID) for joint torque control are known to be sensitive to modeling errors. Hence, pure joint torque control finds its application in robots with closed kinematic chains, e.g., legged robots [16] or open kinematic chains with large inertia compared to the torque inaccuracy. The distal parts of open kinematic chains usually have a small inertia. Therefore, they are often position and velocity controlled in addition to the feedforward torque. In our case, we have a hybrid system. The robot itself is an open kinematic chain. While during therapy, there is always a human arm attached that closes the kinematic chain. We control the

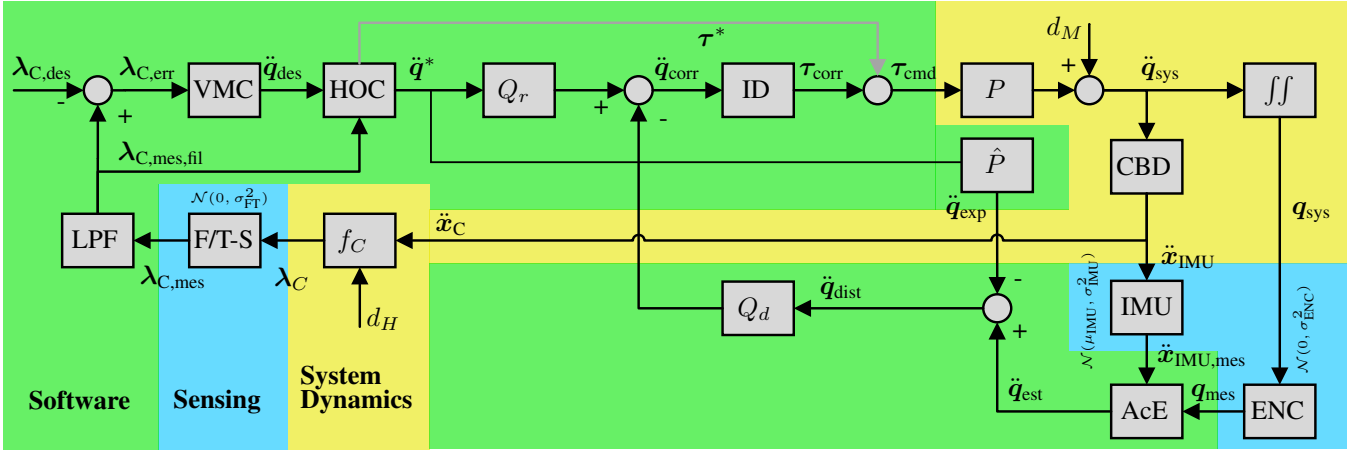


Fig. 2. Control diagram of the virtual mass controller (VMC) with closed loop acceleration control and sensor fusion based acceleration estimation (AcE). The assumed sensor noise for the force-torque sensors (F/T-S), encoder (ENC), and inertial measurement units (IMU) is indicated as gaussian noise. The lowpass filter (LPF) for λ_{mes} is a butter worth filter. The filters for the other sensor signals contained in the AcE. The real system is built from links with finite stiffness. Hence, the IMUs measure the accelerations of the compliant body dynamics (CBD) $\ddot{x}_{\text{IMU},i}$ and not the accelerations equivalent to the mapped joint acceleration $\hat{\ddot{x}}_{\text{IMU},i} = \mathbf{J}_C \ddot{q}_{\text{sys}} + \dot{\mathbf{J}}_C \dot{q}_{\text{sys}}$.

interaction forces over the robot accelerations and assume the human arm to be of rather low impedance. Therefore we expect that the open kinematic chain characteristics of the arm could have a negative influence on the acceleration control. We want to avoid to control all or a subset of the joints in position-control, as we intend to keep the benefits of torque control. Therefore we suggest using an acceleration tracking controller to lower the error.

1) *Controller Synthesis:* We use a 2-DoF *Internal Model Controller* structure for the controller [20]. This controller design includes the plant's model \hat{P} and allows separate tuning of reference tracking Q_r and disturbance rejection Q_d , as shown in Fig. 2. The HOC computes the optimum generalized acceleration \ddot{q}^* as well as optimum actuation torques τ^* . Without the acceleration tracking controller we use the torques from HOC directly as torque commands for the actuators $\tau_{\text{cmd}} = \tau^*$. If we want to correct for errors d_m of the modeled plant, τ^* has to be augmented by the term that compensates for the disturbance resulting in τ_{corr} . As mentioned before, we can assume perfect torque sources in the bandwidth of humans. We assume that τ_{corr} does not contain higher frequency content. Therefore the plant P including the ID can be modelled as pure delay $\hat{P} = e^{-T_s s}$, were T_s is the sampling time.

To assume perfect torque sources without loss of accuracy, Q_r and Q_d need a cutoff frequency lower than the actuator bandwidth. This requirement is feasible, as the human bandwidth is much lower. Reference and disturbance tracking controllers are synthesized as H_2 *Optimal Controller* for ramp references and disturbances as the model errors are mostly continuous (see [20]). Hence, we assume the model disturbance to be of type $\hat{d}_M = 1/s^2$. Applying the methods in [20] to our assumptions results in following control synthesis

$$\begin{aligned} \hat{P} &= e^{-T_s s} \approx \frac{-s + 2/T_s}{s + 2/T_s} \\ \hat{Q}_i &= (\hat{d}_M)^{-1} \{ \hat{P}^{-1} \hat{d}_M \}_* = T_s s + 1 \end{aligned} \quad (9)$$

The operator $\{\cdot\}_*$ omits all terms of the operand's partial fraction expansion that contain the poles of \hat{P}^{-1} . For causality, the controller needs a filter F_i that yields a proper controller $Q_i = \hat{Q}_i F_i$ for $i \in \{d, r\}$. Further, $(1 - \hat{P} Q_i) d_M$ must be stable to reject disturbances asymptotically. The filters F_i are synthesized according to [20]

$$F_i = \frac{a_{k-1} s^{k-1} + \dots + a_1 + a_0}{(\Lambda_i s + 1)^{m+k-1}} = \frac{2\Lambda_i s + 1}{(\Lambda_i s + 1)^2}, \quad i \in \{d, r\}, \quad (10)$$

where $m = 1$ and $k = 2$ as the controller has a zero-pole excess of 1 and d_M has double poles at the origin. The time constants Λ_d and Λ_r for disturbance rejection and reference tracking respectively can be tuned independently.

2) *Acceleration Estimation:* The quality of the acceleration estimation restricts the maximum performance of the acceleration tracking. Typically a system acceleration estimate \hat{q}_{diff} is derived by double differentiation of the joint position measurements. A low pass filter with a low cutoff frequency and a large delay has to be used to attenuate the dominant noise of the signal resulting in \hat{q}_{diff} . We strive for prompt correction of acceleration errors, hence this delay is not acceptable. Therefore, we use the integrated IMUs to measure the system acceleration directly. First, the measured gravitational acceleration of the IMU signals is compensated. Then, the linear accelerations are fused to an estimate of the generalized accelerations using least squares.

$$\begin{aligned} \ddot{x}_{\text{IMU},i,\text{noG}} &= \ddot{x}_{\text{IMU},i} - \mathbf{R}_{\text{IMU},i} \mathbf{g} \\ \hat{\ddot{q}}_{\text{IMU}} &= \mathbf{J}_{\text{IMU}}^+ (\ddot{x}_{\text{IMU},\text{noG}} - \dot{\mathbf{J}} \dot{\mathbf{q}}), \end{aligned} \quad (11)$$

where $\mathbf{R}_{\text{IMU},i}$ is the rotation from inertial coordinates to IMU frame, \mathbf{g} is the gravity vector, and \mathbf{J}_{IMU} and \ddot{x}_{IMU} are the stacked Jacobian respectively acceleration measurements of all IMUs.

Inaccuracies of IMU pose and calibration can lead to severe artifacts of the gravity in the acceleration measurement. Therefore, $\hat{\ddot{q}}_{\text{IMU}}$ is not qualified as control feedback. However, if we merge the information of the delayed (t_{delay}), bias-free \hat{q}_{diff} and the high bandwidth, bias polluted $\hat{\ddot{q}}_{\text{IMU}}$ we

generate an eligible signal. The bias of the latter signal can be estimated by the former which allows compensation

$$\hat{\mathbf{q}}_{\text{bias}}(t) = \hat{\mathbf{q}}_{\text{IMU}}(t - t_{\text{delay}}) - \hat{\mathbf{q}}_{\text{diff}}(t). \quad (12)$$

The high frequency content of the estimated bias $\hat{\mathbf{q}}_{\text{bias}}$ is attenuated with a butterworth filter. The resulting signal $\hat{\mathbf{q}}_{\text{bias,fil}}$ is used to compensate the bias

$$\hat{\mathbf{q}}_{\text{merge}} = \hat{\mathbf{q}}_{\text{IMU}} - \hat{\mathbf{q}}_{\text{bias,fil}}. \quad (13)$$

A further butterworth filter is used to prune the merge estimate from undesired high frequency content.

V. EXPERIMENTS

In this section, we discuss the general procedure for the experiments, while section VI contains specific information. We plan a shoulder synergy controller for the shoulder girdle movement GPR and GED in the future. Therefore, they are locked mechanically for all experiments to avoid interference. Before every experiment with a new parameter set or controller, the software measures and calibrates the F/T-sensors bias to avoid any effect of sensor drift.

After the first couple of experiments, we observed that eigenmodes of the base structure are excited by the strong reaction forces at the attachment point of the arm. To avoid a restriction of the performance by the base's flexibility, we use lashing straps to brace the aluminum beam structure to the floor and ceiling.

A. Acceleration Tracking

For these experiments, we moved the robot to a central position of the RoM. Sinusoidal signals of different amplitudes and frequencies set the reference. All joints use the same controller with individually tuned parameters. The controller is started from a static system by a button on a handheld device.

Stick friction is a challenge for acceleration tracking as the dynamics are entirely different than for the moving system. On the one hand, the system should overcome the stick friction as quickly as possible when acceleration is desired. On the other hand, the disturbance estimation should not wind up on acceleration measurement errors when no motion is requested. Therefore, we use a case differentiation to switch between suitable controller parameters.

B. Interaction Force Control

For all experiments $\lambda_{\text{C,des}} = \mathbf{0}$ is used. During each experiment, one of the authors excited the device by grasping it at the two contact points. This is not the typical way of interaction with an exoskeleton. However, it is easier to achieve repeatable interaction characteristics f_C , as the alignment of human and robot joints is avoided. Furthermore, experiments for parameter tuning can be performed quicker and with less required safety precautions. The presented methods should be transferable to any robot interaction with low impedance environments. Therefore the used type of excitation is as representative as wearing the device like an exoskeleton.

For each controller, we excited the robot as versatile as possible to check the performance. We included collisions with the mechanical end stops to check the stability of the controller. However, the data used to compare the controller is from a repeated movement, which excites all joints without touching the endstops. The movement can be described as a punch from the hip to a point in front of the chest at the height of the shoulders with internal rotation of the shoulder. The test subject repeated this motion while trying to maintain the speed and trajectory throughout all experiments. However, small deviations of the execution are not restricting the validity of the comparison as all metrics are normalized w.r.t. the excitation. The attached video¹ shows examples of the excitation.

VI. RESULTS

The performed experiments and presented results should give an insight into the sensors' characteristics as well as demonstrate and compare the performance of the control methods.

A. Instrumentation Characteristics

The interaction force sensors are calibrated before every experiment. Therefore we assume the bias $\mu_{\text{FT}} = 0$. The variance on the sensor signal was measured over 6s while the device is active but static resulting in following model of the disturbance $d_{\text{FT,force,x}} = \mathcal{N}(0, 0.011)$, $d_{\text{FT,force,yz}} = \mathcal{N}(0, 0.019)$, $d_{\text{FT,torque,x}} = \mathcal{N}(0, 9e - 7)$, and $d_{\text{FT,torque,yz}} = \mathcal{N}(0, 8e - 6)$. The signal is approximately white noise up to 100 Hz where the power falls off until 250 Hz to be constant up to 400 Hz.

The variance in linear acceleration magnitude is in average $\sigma_{\text{IMU}}^2 = 3.6 \times 10^{-4} \text{ m s}^{-4}$ without large variation between the sensors. The bias ranges between $|\mu_{\text{IMU,GED}}| = 0.258 \text{ m s}^{-2}$ and $|\mu_{\text{IMU,GHA}}| = 0.035 \text{ m s}^{-2}$. Correcting for the linear acceleration magnitude bias only would not solve the problem as the IMU axes have an individual scaling error. Furthermore, angular offsets of the IMU mounting of more than 1.5° are expected. Calibration of all axes would be a non-negligible effort. Therefore we introduced the acceleration estimation method using the online bias adaptation.

B. Acceleration Estimation

Fig. 3a) illustrates the main mechanics of the AcE. On the big scope, we can observe how the estimated offset corrects for the configuration dependent bias of $\hat{\mathbf{q}}_{\text{IMU}}$ resulting in an accurate estimation of the acceleration. As ground truth we use the smoothed (non-causal gaussian filter) $\hat{\mathbf{q}}_{\text{diff,smo}}$. The detail view shows how the bias estimation regulates the static offset, which would be devastating for controls.

To demonstrate the performance of the estimation Fig. 3b) shows the estimated signals compared to the ground truth signal. The estimated acceleration describes the acceleration of the compliant body dynamics lumped to the generalized coordinates, while the ground truth shows only the

¹<https://youtu.be/zvz8x3bI8K8>

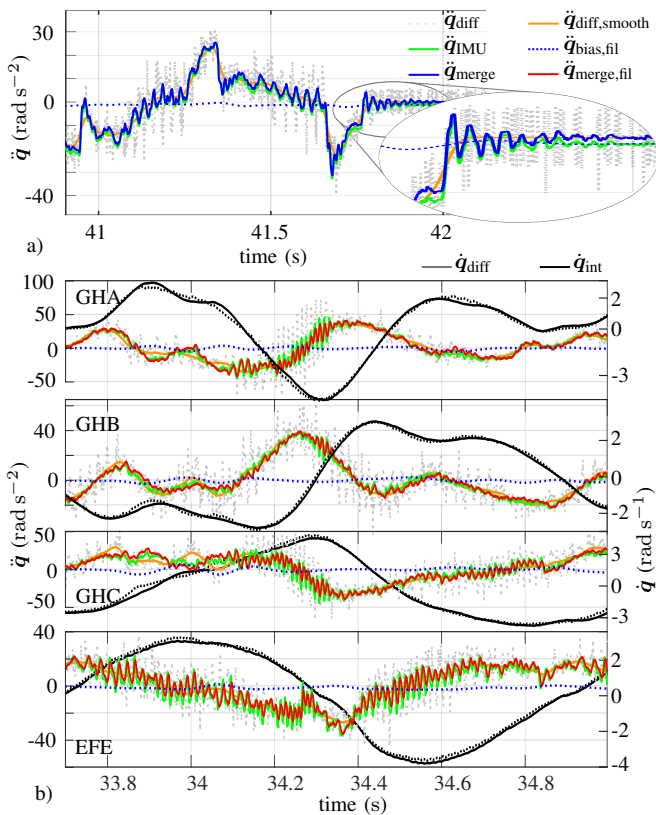


Fig. 3. a) The plot shows the behavior of the acceleration estimation variables during external excitation. The smoothed double-differentiated joint position $\hat{q}_{\text{diff,smo}}$ is used as a reference. Note that the oscillations in the estimated signal are physical compliant body oscillations and not noise. b) shows joint acceleration estimation state of all used joints during a multi-DoF movement and the integrated joint velocities $\hat{q}_{\text{int}} = \int \hat{q}_{\text{merge}} dt$ after more than 15 s run time.

acceleration of the joints. Hence, the continuum mechanics of the links are missing in the ground truth, which could explain the momentaneous differences. In the integrated \hat{q}_{merge} , these differences should not lead to drift, as the compliant body dynamics are only oscillations around the rigid body dynamics. The black signals in Fig. 3b) show the integrated velocity compared to the measured after more than 15 s run time. There is no drift, proving the method to be valid.

C. Acceleration Tracking

Joint EFE is the most critical one regarding inverse dynamics as its output is attached to a low inertia. Therefore dynamic and static friction are large compared to the torques needed for acceleration. Fig. 4a) and b) show the effect of an active joint acceleration control with $\Lambda_r = 0.01$ and $\Lambda_d = 0.09$. While the joint does not move without acceleration control, it follows the desired trajectory well with active control. The influence of the stick friction handling is particularly distinct.

The estimated disturbance for EFE, GHB, and GHC in 4b)-c) shows completely different characteristics. The disturbance is specific to the actuator, the six-DoF joint load, and even the internal temperature. The estimation indicates how complex a model would have to be to calibrate the

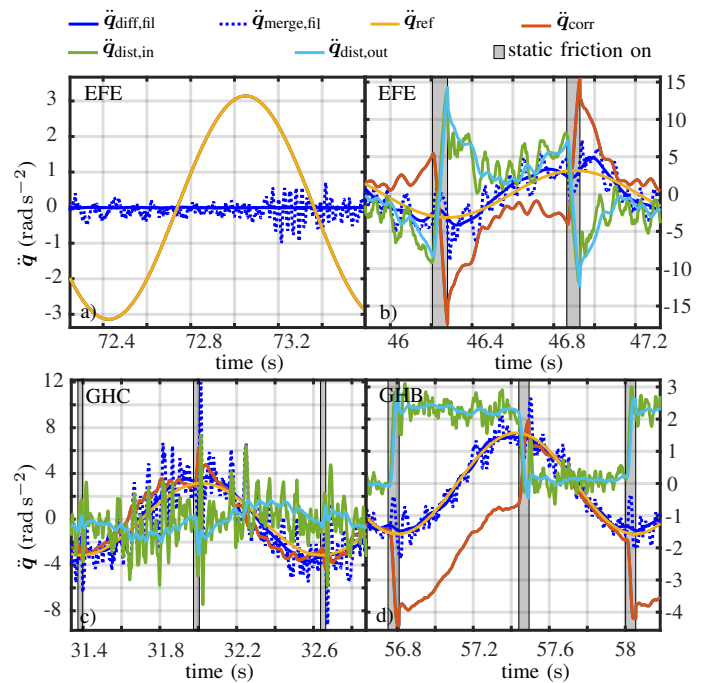


Fig. 4. The four plots show the tracking performance w.r.t. a sinusoidal reference acceleration \hat{q}_{ref} . Plot a) shows the performance without active ATC and b) with ATC for the same reference trajectory on the EFE joint. Plots b), c), and d) show the tracking controller state on different joints.

disturbance offline.

D. Interaction Force Tracking

The open-loop controller (FF) described in equation (5) with $\ddot{q}^* = 0$ and $\lambda_{C,\text{des}} = 0$ is used as a baseline. In the publication about the hardware [6], we compared the performance of the device against the state of the art [10]. The results of [6] indicate, that the controller achieves haptic transparency that is on par with the state of the art and is potentially superior for dynamic movements.

We evaluate the performance of the controller with different metrics that should represent transparency as accurately as possible for a wide variety of excitations. The test subject cannot excite the robot the same in each experiment run. Therefore, all metrics are as independent of the excitation as possible. As such normalized metrics were missing in the state-of-the-art [10], we introduced new ones.

Inertia Ratio \mathcal{IR} describes the ratio of felt inertia at one joint to the reflected inertia of the physical system at the same joint. Thus, small numbers indicate accurate wrench tracking.

$$\mathcal{IR}_i = \frac{m_{\text{virt}}}{m_{\text{sys}}} = \frac{\mathbf{S}_i \mathbf{J}_C^T \lambda_{C,\text{mes}}}{\mathbf{S}_i \mathbf{M} \ddot{\mathbf{q}}_{C,\text{mes}}} \quad (14)$$

where \mathbf{S}_i is the selection vector of DoF i . Both denominator and nominator of the equations (14) are smoothed. $\mathcal{IR}_{i,\text{mean}}$ is the mean over time for DoF i . $\mathcal{IR}_{\text{mean}}$ is the mean of all $\mathcal{IR}_{i,\text{mean}}$.

Inertia Ratio Span $\Delta \mathcal{IR}$ indicates the consistency of virtual mass rendering.

$$\Delta \mathcal{IR} = \max_i(\mathcal{IR}_{i,\text{mean}}) - \min_i(\mathcal{IR}_{i,\text{mean}}). \quad (15)$$

TABLE I

COMPARISON OF INTERACTION WRENCH CONTROL METHODS. FEED FORWARD COMPENSATION (FF) OF THE DYNAMICS. VIRTUAL MASS CONTROL (VMC) WITHOUT CLOSED LOOP ACCELERATION TRACKING AND (VM+ATC) WITH ACCELERATION TRACKING CONTROLLER. ALL DATA IS AVERAGED FROM CONTINUOUS SAMPLES OF AT LEAST 10 s. †:

THIS IS THE MEAN OF JOINTS GHA, GHB, AND GHC.

| Method | FF | VMC | VMC | VM+ATC | VM+ATC | VM+ATC |
|--|------|------|------|--------|--------|--------|
| α | - | 0.7 | 0.6 | 0.7 | 0.7 | 0.6 |
| Λ_r | - | - | - | 0.01 | 0.01 | 0.01 |
| Λ_d | - | - | - | 0.14 | 0.19 | 0.14 |
| $\overline{\mathcal{I}\mathcal{R}}_{\text{mean,GH}}^\dagger$ | 1.51 | 0.51 | 0.51 | 0.52 | 0.52 | 0.49 |
| $\overline{\mathcal{I}\mathcal{R}}_{\text{mean}}$ | 1.76 | 0.59 | 0.58 | 0.56 | 0.57 | 0.52 |
| $\Delta\overline{\mathcal{I}\mathcal{R}}_{\text{mean}}$ | 1.13 | 0.34 | 0.34 | 0.24 | 0.27 | 0.19 |
| $\overline{\mathcal{T}\mathcal{R}}_{\text{mean}}$ | 1.12 | 0.46 | 0.46 | 0.45 | 0.47 | 0.41 |

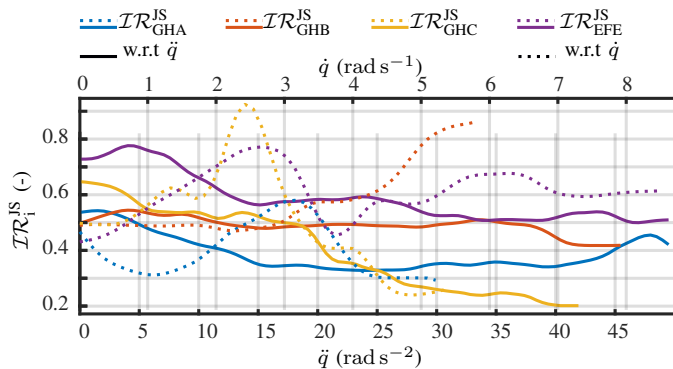


Fig. 5. The average inertia ratio at a certain joint acceleration and joint speed is plotted in this figure for all controlled joints.

Peak Torque Ratio $\overline{\mathcal{T}\mathcal{R}}$ describes the ratio peak interaction torque to the peak expected interaction torque.

$$\overline{\mathcal{T}\mathcal{R}}_i = \frac{\max(\tau_{\text{virt}})}{\max(\tau_{\text{sys}})} = \frac{\max(\mathbf{S}_i \mathbf{J}_C^T \boldsymbol{\lambda}_{C,\text{mes}})}{\max(\mathbf{S}_i \mathbf{M} \ddot{\mathbf{q}}_{\text{mes}})}. \quad (16)$$

1) *Scalar Excitation-Normalized Metrics*: In Table I these scalar metrics are compared for the different methods using control parameters that have shown best performance during systematic tuning. We can observe that our proposed controllers VMC and VM+ATC reduce the inertia ratio $\overline{\mathcal{I}\mathcal{R}}$ by a factor of three compared to the baseline controller FF. The variation of the inertia ratio $\Delta\overline{\mathcal{I}\mathcal{R}}$ is lowered by a factor of six for the best method. The peak torque ratio is also reduced by more than a factor of two by all proposed methods. Hence, the proposed controllers are superior to the baseline. The VM+ATC controllers seem to perform slightly better in reducing the $\Delta\overline{\mathcal{I}\mathcal{R}}$. However, in the $\overline{\mathcal{I}\mathcal{R}}$ metric, there is no relevant difference observable.

2) *Velocity and Acceleration Sensitivity*: To render an intuitive feeling of free space, it is vital to see if the system behaves consistently over the full bandwidth of accelerations. Figure 5 shows the average $\overline{\mathcal{I}\mathcal{R}}_{\text{mean}}$ at different accelerations. The rendered impedance is quite consistent. A clear drop in $\overline{\mathcal{I}\mathcal{R}}_{\text{mean,GHC}}$ is observable for higher accelerations as well as a peak around 2.3 rad s^{-2} . This can be explained by a very low amount of data at this velocity and acceleration in our experiments. Hence, these deviations might be a specific artifact of the chosen excitation.

TABLE II

PERFORMANCE OF VMC AND VM+ATC CONTROLLER IN THE PRESENCE OF A LARGE MASS MODELLING ERROR OF THE UPPER ARM

LINK $\Delta m_{\text{UA}} = -1 \text{ kg}$.

| Method | VMC | VM+ATC | VMC | VM+ATC |
|---|------|--------|------|--------|
| α | 0.7 | 0.7 | 0.6 | 0.6 |
| Λ_r | - | 0.01 | - | 0.01 |
| Λ_d | - | 0.14 | - | 0.14 |
| $\overline{\mathcal{I}\mathcal{R}}_{\text{mean}}$ | 0.60 | 0.53 | 0.55 | 0.50 |
| $\Delta\overline{\mathcal{I}\mathcal{R}}_{\text{mean}}$ | 0.67 | 0.09 | 0.18 | 0.16 |
| $\overline{\mathcal{T}\mathcal{R}}_{\text{mean}}$ | 0.50 | 0.49 | 0.38 | 0.46 |

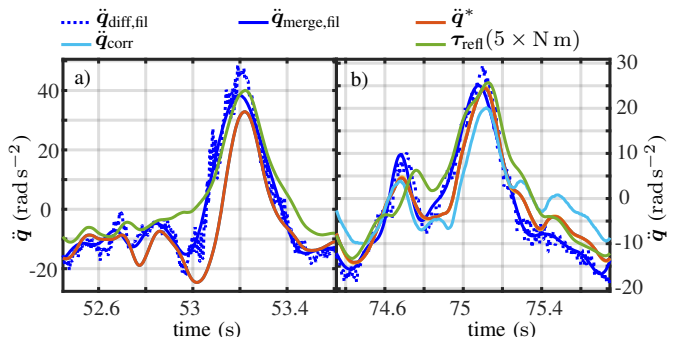


Fig. 6. Interaction wrench tracking performance at joint GHB under a mass model error of -1 kg at the exoskeleton's upper arm. The results are shown without a) and with b) acceleration control. The reflected torque is $\tau_{\text{ref}} = \mathbf{J}_C^T \boldsymbol{\lambda}_C$. Further, $\ddot{\mathbf{q}}^* = \ddot{\mathbf{q}}_{\text{ref,out}}$.

3) *Robustness Against Modelling Errors*: We assess the robustness of the control methods by inducing a large mass modeling error for the upper arm link $\Delta m_{\text{UA}} = -1 \text{ kg}$. Table II shows the resulting differences using the scalar values. The results are shown for the control parameter sets which have shown best performance in for the nominal model. Both controllers show a quite good performance while the acceleration tracking seems to improve the performance slightly. Figure 6 shows the improved acceleration reference tracking performance. The improved tracking helps to render a more consistent feeling of low inertia as the system behaves more like the controller dictates. This can be explained by the ATC compensating for $\Delta\boldsymbol{\lambda}_C$ in equation (8). Without the ATC, the interaction feels very transparent during high jerk as $\Delta\boldsymbol{\lambda}_C$ helps to accelerate the system. However, when the jerk crosses zero, the inertia feels higher than with ATC.

VII. DISCUSSION & CONCLUSION

We presented a control method to render free motion with a multi-DoF rehabilitation exoskeleton in the presence of rapid and high-acceleration movements by the user. We proposed to compensate for the device's dynamics as accurately as possible during these swift movements. Therefore, we propose to work with the best knowledge of the current system state to feedback linearize the dynamics at the interaction points to the user. We introduce a controller rendering a low virtual mass (VMC) at the end-effector by converting the measured interaction wrench to desired accelerations.

To further improve the performance in the presence of model inaccuracies, we developed a closed-loop joint acceleration controller (ATC). Therefore, we introduced a method to fuse the double differentiated joint encoder signals and

acceleration measurements from multiple low priced IMUs to an estimation of the generalized joint acceleration. This estimate was shown to be bias-free and to have a low delay, which makes it eligible for feedback control. We could demonstrate that the feedback acceleration control improves the tracking performance significantly. Particularly for joints with low attached inertia, this method is recommendable if position control is not an option. Furthermore, the method uses affordable IMUs, which keeps the hurdle for a transfer to other robots low. An experimental comparison of the proposed approach's performance to state-of-the-art methods that do not use \ddot{q} to estimate the tracking error, as presented in [21] and [10], should be addressed in future research.

Further, we compared variations of the method w.r.t. each other and against a model-based feedforward controller as a reference. In an earlier publication, this reference method showed performance on par with state-of-the-art closed loop controllers on comparable devices. The experiments demonstrated that the introduced method is significantly superior regarding all considered performance metrics compared to the reference controller. The felt inertia, as well as the maximum felt joint torque, could be reduced by more than a factor of three. Besides, the method showed robust behavior in the presence of significant modeling errors.

With the non-integrative VMC, we could demonstrate that the inverse dynamics with the best momentary model approach is a promising method to lay the ground for linear interaction wrench controller synthesis. We intend to extend the method using controllers with integrative action or/and prior knowledge about the environment's impedance (e.g., human) to improve the performance further.

These results set a new benchmark for dynamic free space rendering in rehabilitation exoskeletons. It is possible to employ this method in combination with hierarchical optimization strategies, which allows one to intuitively combine it with tasks on other priorities, e.g., position limits. Therefore, the VMC is used as a new standard on the rehabilitation exoskeleton ANYexo. The level of transparency should pave the way for novel intervention techniques in neurorehabilitation. The results indicate that the proposed multi-sensor based closed-loop acceleration tracking improves the accuracy of the inverse dynamics. This method is attractive for all inverse dynamics applications and particularly for joints with low attached inertia. The presented control methods, as well as the findings of the experiments, should be well transferable to end-effector type haptic devices as well as for manipulators to delicately interact with general environments that have an unknown low impedance.

ACKNOWLEDGMENT

This research was supported in part by the Swiss National Science Foundation (SNSF) through the National Centre of Competence in Research Robotics (NCCR Robotics) and Innosuisse the Swiss Innovation Agency. Furthermore, we would like to thank Konrad Meyer, Klajd Lika, Ilias Patsiaouras, Markus Stäubli, Fabian Just, and others from

the Robotic Systems Lab, Sensory-Motor Systems Lab, and ANYbotics for their relentless support of the project.

REFERENCES

- [1] T. Proietti, V. Crocher, A. Roby-Brami, and N. Jarrasse, "Upper-limb robotic exoskeletons for neurorehabilitation: A review on control strategies," 2016.
- [2] A. Otten, C. Voort, A. Stienen, R. Aarts, E. Van Asseldonk, and H. Van Der Kooij, "LIMPACT: A Hydraulically Powered Self-Aligning Upper Limb Exoskeleton," *IEEE/ASME Transactions on Mechatronics*, 2015.
- [3] R. A. Gopura, D. S. Bandara, K. Kiguchi, and G. K. Mann, "Developments in hardware systems of active upper-limb exoskeleton robots: A review," *Robotics and Autonomous Systems*, 2016.
- [4] V. Klamroth-Marganska, J. Blanco, K. Campen, A. Curt, V. Dietz, T. Ettlin, M. Felder, B. Fellinghauer, M. Guidali, A. Kollmar, A. Luft, T. Nef, C. Schuster-Amft, W. Stahel, and R. Riener, "Three-dimensional, task-specific robot therapy of the arm after stroke: A multicentre, parallel-group randomised trial," *The Lancet Neurology*, 2014.
- [5] M. Ferreira, M. Emi, A. Chaves, F. Ma, C. Oliveira, A. Maria, C. Bruno, and S. Vimieiro, "Effectiveness of robot therapy on body function and structure in people with limited upper limb function : A systematic review and meta-analysis," *PlosOne*, 2018.
- [6] Y. Zimmermann, A. Forino, R. Riener, and M. Hutter, "ANYexo: A Versatile and Dynamic Upper-Limb Rehabilitation Robot," *IEEE Robotics and Automation Letters*, oct 2019.
- [7] T. Nef, M. Guidali, and R. Riener, "ARMin III – arm therapy exoskeleton with an ergonomic shoulder actuation," *Applied Bionics and Biomechanics*, vol. 6, no. 2, pp. 127–142, 2009.
- [8] B. Kim and A. D. Deshpande, "An upper-body rehabilitation exoskeleton Harmony with an anatomical shoulder mechanism: Design, modeling, control, and performance evaluation," *The International Journal of Robotics Research*, 2017.
- [9] H. Vallery, J. Veneman, E. van Asseldonk, R. Ekkelenkamp, M. Buss, and H. van Der Kooij, "Compliant actuation of rehabilitation robots," *IEEE Robotics and Automation Magazine*, 2008.
- [10] F. Just, Ö. Özen, P. Bösch, H. Bobrovsky, V. Klamroth-Marganska, R. Riener, and G. Rauter, "Exoskeleton transparency: feed-forward compensation vs. disturbance observer," at - *Automatisierungstechnik*, 2018.
- [11] F. Farshidian, E. Jelavic, A. W. Winkler, and J. Buchli, "Robust whole-body motion control of legged robots," *IEEE International Conference on Intelligent Robots and Systems*, 2017.
- [12] Y. Mao and S. K. Agrawal, "Design of a cable-driven arm exoskeleton (CAREX) for neural rehabilitation," *IEEE Transactions on Robotics*, 2012.
- [13] J. C. Perry, J. Rosen, and S. Burns, "Upper-limb powered exoskeleton design," *IEEE/ASME Transactions on Mechatronics*, 2007.
- [14] M. Hutter, C. Gehring, D. Jud, A. Lauber, C. D. Bellicoso, V. Tsounis, J. Hwangbo, P. Fankhauser, M. Bloesch, R. Diethelm, and S. Bachmann, "ANYmal - A Highly Mobile and Dynamic Quadrupedal Robot," submitted to *IEEE/RSJ International Conference on Intelligent Robots and Systems (IROS)*, 2016.
- [15] T. L. Brooks, "Telerobotic response requirements," *Systems, Man and Cybernetics, 1990. Conference Proceedings., IEEE International Conference on*, 1990.
- [16] C. Dario Bellicoso, C. Gehring, J. Hwangbo, P. Fankhauser, and M. Hutter, "Perception-less terrain adaptation through whole body control and hierarchical optimization," in *IEEE-RAS International Conference on Humanoid Robots*, 2016.
- [17] T. Horibe, E. T. B., and R. B. Gillespie, "Comparing Series Elasticity and Admittance Control for Haptic Rendering," *EuroHaptics 2016*, 2016.
- [18] C. Carignan and K. Cleary, "Closed-loop force control for haptic simulation of virtual environments," *Haptics-e*, feb 2000.
- [19] N. Hogan, "Impedance control: An approach to manipulation: Part I-theory," *Journal of Dynamic Systems, Measurement and Control, Transactions of the ASME*, vol. 107, no. 1, pp. 1–7, mar 1985.
- [20] M. Morari, "Robust Process Control," *Chemical Engineering Research and Design*, 1987.
- [21] S. Haddadin, A. De Luca, and A. Albu-Schäffer, "Robot collisions: A survey on detection, isolation, and identification," *IEEE Transactions on Robotics*, vol. 33, no. 6, pp. 1292–1312, 2017.